PHYSICAL REVIEW D **92,** 014001 (2015)

Single-inclusive production of hadrons and jets in lepton-nucleon scattering at NLO

Patriz Hinderer,[*] Marc Schlegel,[†] and Werner Vogelsang[‡]

Institute for Theoretical Physics, Universität Tübingen, Auf der Morgenstelle 14, D-72076 Tübingen, Germany

(Received 1 June 2015; published 2 July 2015)

We present next-to-leading order (NLO) perturbative-QCD calculations of the cross sections for $\ell N \to hX$ and $\ell N \to \text{jet}X$. The main feature of these processes is that the scattered lepton is not observed, so that the hard scale that makes them perturbative is set by the transverse momentum of the hadron or jet. Kinematically, the two processes thus become direct analogs of single-inclusive production in hadronic collisions which, as has been pointed out in the literature, makes them promising tools for exploring transverse spin phenomena in QCD when the incident nucleon is transversely polarized. We find that the NLO corrections are sizable for the spin-averaged cross section. We also investigate in how far the scattering is dominated by the exchange of almost real (Weizsäcker-Williams) photons. We present numerical estimates of the cross sections for present-day fixed target experiments and for a possible future electron-ion collider.

DOI: 10.1103/PhysRevD.92.014001 PACS numbers: 12.38.Bx, 13.60.Hb, 13.85.Ni

I. INTRODUCTION

There has been growing interest recently, both experimentally [1–4] and theoretically [5–10], in the processes $\ell N \to hX$ and $\ell N \to \text{jet}X$, the single-inclusive production of a hadron or jet at large transverse momentum in lepton-nucleon scattering. In contrast to the far more customary process $\ell N \to \ell' hX$ [11], for $\ell N \to hX$ the scattered lepton in the final state is not observed, so that the process is truly one-hadron (or one-jet) inclusive. The reason for the interest in $\ell N \to hX$ comes from the study of single-transverse-spin phenomena in hadronic scattering processes. It is well known that large single-spin asymmetries have been observed [12] for the process $pp^\uparrow \to hX$, where $p^\uparrow$ denotes a transversely polarized proton. To explain the large size of the asymmetries, and their persistence all the way from fixed-target to collider energies, has posed a major challenge to theory. Although a lot has been learned, it is fair to say that a fully satisfactory understanding has yet to be obtained. Measurements of corresponding asymmetries in the kinematically equivalent, but much simpler, processes $\ell N^\uparrow \to hX$, $\ell N^\uparrow \to \text{jet}X$ have the promise of shedding new light on the mechanisms for single-spin asymmetries in QCD. First fairly precise experimental data for $\ell N^\uparrow \to hX$ have recently been released by the HERMES [2,3] and Jefferson Lab Hall A [4] collaborations.

We note that at first sight one might consider the related process $\ell N^\uparrow \to \ell' X$ [which is just the standard inclusive deep-inelastic scattering (DIS) process] to be equally suited for transverse-spin studies in lepton scattering. However, the analysis of the corresponding single-spin asymmetry is considerably more complex because higher-order QED effects are required for the asymmetry to be nonvanishing [13–17]. In the same spirit as $\ell N^\uparrow \to hX$, also the processes $\vec{\ell} N^\uparrow \to hX$ [18] with longitudinal polarization of the lepton and $\ell N \to \Lambda^\uparrow X$ [19] with a transversely polarized Λ hyperon were considered in the literature recently.

The proven method for analyzing single-inclusive processes such as $pp \to hX$ or $\ell N \to hX$ at large transverse momentum rests on QCD perturbation theory and collinear factorization. For single-transverse-spin observables, this involves a twist-3 formalism in terms of three-parton correlation functions of the nucleon or the fragmentation process [20–29]. Interestingly, the recent study [29] suggests that the twist-3 fragmentation effects could be the dominant source of the observed large transverse-spin asymmetries in $pp^\uparrow \to hX$. An alternative approach for describing the single-spin asymmetry in inclusive hadron production in $pp^\uparrow \to hX$ was devised in the context of a "generalized" parton model in which the dependence of parton distributions and fragmentation functions on transverse momentum is kept [30–32]. Although no such factorization in transverse momentum is known to be valid for a single-inclusive cross section, the approach has enjoyed considerable phenomenological success.

Both the collinear twist-3 approach and the generalized parton model have been used to obtain predictions for the spin asymmetry in $\ell N^\uparrow \to hX$. In Ref. [7] a leading order (LO) twist-3 analysis has been presented in terms of parton correlation functions that were previously extracted from data for $pp^\uparrow \to hX$. The results obtained in this way fail to describe the HERMES data [2,3] for the spin asymmetries in $\ell N^\uparrow \to hX$. A comparison of perturbative calculations to the corresponding JLab data [4] is not possible as the data

[*]patriz.hinderer@uni-tuebingen.de
[†]marc.schlegel@uni-tuebingen.de
[‡]werner.vogelsang@uni-tuebingen.de

 © 2015 American Physical Society

are for hadrons with transverse momenta below 1 GeV. The LO generalized parton model approach, on the other hand, appears to give results quite consistent with the HERMES data [8–10].

In our view it is premature to draw any conclusions from these findings at LO. Given the kinematics (and the precision) of the present data, one may expect higher-order QCD corrections to the cross sections and the asymmetry to be important [7] for a meaningful comparison of data and theory. At least next-to-leading order (NLO) corrections should be included. We stress that the twist-3 formalism, although so far only developed to LO, offers a well-defined framework for a perturbative study of the transverse-spin asymmetry in $\ell N^\uparrow \to hX$. This is in contrast to the generalized parton model, for which there is likely no systematic way of going to higher orders in perturbation theory. That said, NLO calculations within the twist-3 formalism are technically very challenging, and only a few NLO calculations have been performed for the simpler Drell-Yan [33] and semi-inclusive DIS cases [34].

In the present paper, we take a first step toward a NLO calculation of the transverse-spin asymmetry for $\ell N^\uparrow \to hX$ by computing the NLO corrections to the spin-averaged cross section for the process, which constitutes the denominator of the spin asymmetry. We present analytical results for the NLO partonic cross sections. To our knowledge, despite the vast amount of work performed for lepton proton scattering in the literature (see, for example [35–41]), this calculation has not been presented so far. We also present similar NLO calculations for the process $\ell N \to \text{jet}X$. We note that the process $\ell N \to \text{jet}X$ has also been extensively studied in terms of the concept of "1-jettiness" [42,43]. Here one additionally writes the cross section differential in a variable τ_1 that characterizes the hadronic final state that is *not* associated with the produced jet or the nucleon beam remnant. In Ref. [43] the full NLO corrections for the 1-jettiness were computed, where a fully numerical approach was adopted. In principle, it should be possible to recover our NLO results by performing a (numerical) integration over τ_1 of the results of [43].

Because of the propagator of the exchanged photon, the cross section for $\ell N^\uparrow \to hX$ will contain contributions for which the photon is almost on shell. This is not yet the case at LO where the high transverse momentum of the produced hadron requires the photon to be highly virtual. Starting from NLO, however, it may happen that the incoming lepton radiates the photon almost collinearly. This may then be followed by a $2 \to 2$ scattering process of the photon with a parton in the nucleon, which is perfectly capable of producing the hadron at high $P_{h\perp}$. In processes where the scattered lepton is observed, such as $\ell N \to \ell' hX$, one can in fact select such contributions by requiring the scattered lepton to have a low scattering angle. The incoming lepton then effectively acts merely as a source of quasireal photons, and the process may be very accurately described in terms of a (perturbative) distribution function for photons in leptons known as the Weizsäcker-Williams (WW) distribution [11,44–47]. This approach has been widely used with much success in the HERA physics program [11].

In the context of our NLO calculation for $\ell N \to hX$ it is therefore interesting to investigate whether also in this case the contributions by almost real photons dominate and the NLO corrections may be well approximated by a Weizsäcker-Williams-type distribution. Since it is much easier to compute the latter contribution than the full NLO correction, this would mean that one could also obtain approximate NLO results for the transversely polarized cross section within the twist-3 framework by simply considering real photons. Given the complexity of a full NLO calculation for the twist-3 case, this would be a tremendous advantage. We note that the contributions to the spin-dependent cross sections for $\ell N \to \text{jet}X$ for real photons were discussed in [6], including the twist-3 contributions for the single-transverse-spin case. Actual LO calculations for the twist-2 longitudinal spin-dependent cross section were presented in Ref. [48] for quasireal photons. We will closely examine the contributions by quasireal photons also in our paper. Their relevance will of course also depend on the lepton species that is used, because the lepton mass leads to a lower limit on the virtuality of the photon.

Our paper is structured as follows. In Sec. II we present our NLO calculations for the partonic cross sections for $\ell N^\uparrow \to hX$ and $\ell N \to \text{jet}X$. We also discuss in some detail the Weizsäcker-Williams contribution and how the calculation can be done keeping a finite lepton mass. Section III presents numerical predictions for the NLO cross section to be expected at various fixed-target experiments and at a future electron-ion collider (EIC). Finally, we summarize our results in Sec. IV.

II. NLO CALCULATION

A. General framework

In this section we present our derivation of the analytical NLO results for the processes $\ell N \to hX$ and $\ell N \to \text{jet}X$. The transverse momentum of the produced hadron or jet sets a hard scale, so that perturbative methods may be used for treating the cross sections. We first consider $\ell(l) + N(P) \to h(P_h) + X$, where we have introduced our notation for the four-momenta. It is useful to introduce the Mandelstam variables as $S = (P + l)^2$, $T = (P - P_h)^2$ and $U = (l - P_h)^2$. Furthermore, we label the energy of the detected hadron as E_h and its three-momentum by $\vec{P}_h$.

In collinear leading-twist perturbative QCD the hadronic cross section is approximated by convolutions of hard partonic scattering cross sections and parton distribution/fragmentation functions. The momenta of the incoming parton, k^μ, and of the fragmenting parton, p^μ, which appear

in the calculation of the partonic cross sections, are approximated as $k^\mu \simeq xP^\mu$ and $p^\mu \simeq P_h^\mu/z$, respectively. It is then convenient to work with the partonic Mandelstam variables

$$s = (k+l)^2 = xS,$$
$$t = (k-p)^2 = \frac{x}{z}T,$$
$$u = (l-p)^2 = \frac{U}{z}. \tag{1}$$

The general form of the factorized cross section for the inclusive hadron production process then is

$$E_h \frac{d^3\sigma^{\ell N\to hX}}{d^3P_h} = \frac{1}{S}\sum_{i,f}\int_0^1 \frac{dx}{x}\int_0^1 \frac{dz}{z^2} f^{i/N}(x,\mu) \times D^{h/f}(z,\mu)\hat{\sigma}^{i\to f}(s,t,u,\mu), \tag{2}$$

where $f^{i/N}(x,\mu)$ is the parton distribution function (PDF) for the incoming parton i in the nucleon N and $D^{h/f}(z,\mu)$ the corresponding fragmentation function for parton f fragmenting into hadron h, both evaluated at a factorization scale μ. We choose the factorization scales to be the same for the initial and the final state, and also equal to the renormalization scale. In Eq. (2), $\hat{\sigma}^{i\to f}$ is the partonic cross section for the lepton-parton scattering process, $\ell + i \to f + x$, with x an unobserved partonic final state. The sum in Eq. (2) runs over the different species of partons, quarks, gluons and antiquarks. We note that the expression in Eq. (2) holds up to corrections that are suppressed by inverse powers of the produced hadron's transverse momentum $P_{h\perp}$.

The partonic cross sections $\hat{\sigma}^{i\to f}$ in Eq. (2) can be calculated in QCD perturbation theory. One may write their expansion in the strong coupling as

$$\hat{\sigma}^{i\to f} = \hat{\sigma}^{i\to f}_{\rm LO} + \frac{\alpha_s}{\pi}\hat{\sigma}^{i\to f}_{\rm NLO} + \mathcal{O}(\alpha_s^2). \tag{3}$$

At lowest order only the tree-level process $\ell q \to q\ell$ shown in Fig. 1 contributes. The calculation of its cross section is straightforward. One finds

$$\hat{\sigma}^{q\to q}_{\rm LO} = 2\alpha_{\rm em}^2 e_q^2 \frac{s^2+u^2}{t^2}\delta(s+t+u), \tag{4}$$

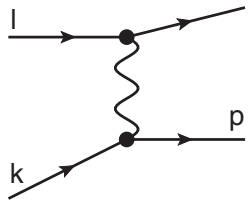

FIG. 1. LO diagram for lepton-quark scattering.

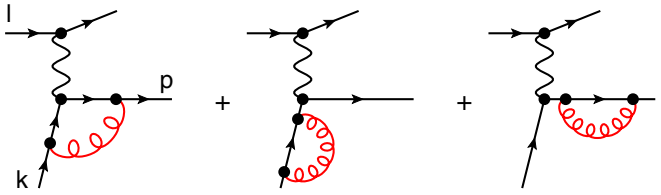

FIG. 2 (color online). Virtual diagrams at NLO. Self-energy diagrams (right and middle graph) contribute in Feynman gauge.

where $\alpha_{\rm em}$ is the fine structure constant and e_q is the quark's fractional charge.

At NLO, $\mathcal{O}(\alpha_s\alpha_{\rm em}^2)$, both virtual (Fig. 2) and real-emission diagrams [Figs. 3(a)–3(c)] contribute. We will address these in turn in the following subsections. One can see from Figs. 3(b) and 3(c) that beyond LO there are also new contributions where a gluon fragments or where an initial gluon enters the hard scattering process.

As is well known, all types of NLO contributions develop singularities at intermediate stages of the calculations, which we make manifest by using dimensional regularization with $D = 4 - 2\varepsilon$ space-time dimensions. The subsequent treatment of the singularities is standard in perturbative QCD (pQCD) calculations. The only nonstandard feature arises for the incoming lepton. If we assume for the moment that we have an incoming quark instead of a lepton in the diagrams in Fig. 3(a) and an exchanged gluon instead of a photon, then the diagram would make a NLO contribution to, say, $pp \to hX$. Being treated as massless, the initial quark would produce a singularity when it radiates the gluon collinearly. As is well understood, this singularity may be absorbed ("factorized") into the proton's quark PDF, exactly in the same way as for the incoming quark at the bottom of the diagram. In the case of an incoming lepton, on the other hand, the lepton's mass ensures that no collinear singularity arises when the lepton radiates a collinear photon that subsequently participates in the hard scattering. In fact, keeping the lepton mass m_ℓ, the cross section will develop a logarithmic term of the form $\alpha_{\rm em}\log(\Lambda/m_\ell)$, where Λ represents a hard scale of the problem, and in the limit $m_\ell \to 0$ this logarithm precisely produces the required collinear singularity. In principle we should therefore perform the NLO calculation keeping the lepton mass finite. This is technically very cumbersome, and in fact not needed. We can adopt two different, and equivalent, approaches instead: In the first approach we neglect the lepton's mass and regularize the ensuing collinear pole in dimensional regularization. The pole is then subtracted (for example, in the $\overline{\rm MS}$ scheme) and absorbed into a "parton" distribution function for photons in a lepton. This distribution may be evaluated perturbatively in first-order QED, giving rise essentially to the well-known "Weizsäcker-Williams" distribution. This approach may in principle be extended to higher order in QED. In the second approach, we calculate the cross section for a massive lepton, keeping however only the leading terms

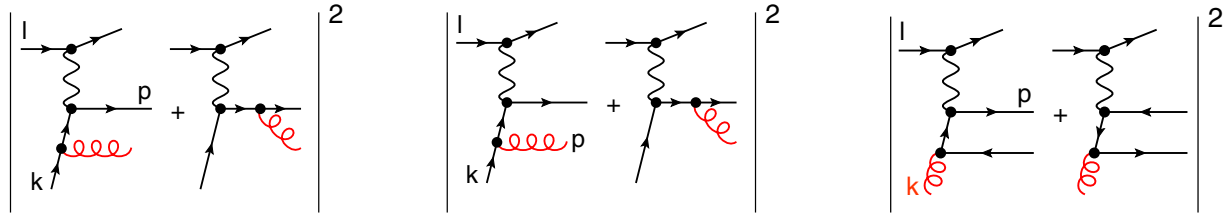

FIG. 3 (color online). NLO real-emission diagrams. There are three partonic channels at NLO: (a) $q \to q$, (b) $q \to g$, (c) $g \to q$.

in m_ℓ which are of the form $\alpha_{\rm em}[\log(\Lambda/m_\ell) + \text{constant}]$. This is justified by the fact that all terms beyond this approximation are suppressed as powers of m_ℓ over the hard scale and hence numerically tiny. We note that although the logarithm can become large (as m_ℓ is small compared to typical QCD hard scales), the smallness of $\alpha_{\rm em}$ will usually make the term $\alpha \log(\Lambda/m_\ell)$ small enough to be regarded as a perturbative correction. We will present our main calculation for the case of massless leptons and comment on the use of a finite lepton mass in the calculation later.

It is convenient to rewrite the x and z integrals in Eq. (2) in terms of new variables $v = 1 + t/s$ and $w = -u/(s+t)$. Using (1), we have

$$x = \frac{1-v}{vw}\frac{U}{T}, \qquad z = \frac{-T}{(1-v)S}, \tag{5}$$

and Eq. (2) becomes

$$E_h \frac{d^3\sigma^{\ell N\to hX}}{d^3P_h} = \left(\frac{-U}{S^2}\right)\sum_{i,f}\int_{\frac{U}{T+U}}^{1+\frac{T}{S}} \frac{dv}{v(1-v)}\int_{\frac{1-vU}{v\,T}}^{1}\frac{dw}{w^2} \times H^{if}(v,w)\hat{\sigma}^{i\to f}(v,w,\mu), \tag{6}$$

where we have defined

$$H^{if}(v,w) \equiv \left.\frac{f^{i/N}(x,\mu)}{x}\frac{D^{h/f}(z,\mu)}{z^2}\right|_{x=\frac{1-vU}{vw\,T}, z=\frac{-T}{(1-v)S}}. \tag{7}$$

For ease of notation, we have kept the symbol $\hat{\sigma}^{i\to f}$ also for the cross section when expressed in terms of the new variables. We note that the invariant mass of the unobserved recoiling partonic final state is given by $s+t+u = sv(1-w)$. The function $\delta(s+t+u) \propto \delta(1-w)$ in the LO cross section (4) expresses the fact that at LO the recoil consists of a single parton.

B. Virtual contributions at NLO

At the NLO level, the virtual contributions shown in Fig. 2 contribute through their interference with the Born diagram. The virtual contributions thus have Born kinematics and are proportional to $\delta(1-w)$. Since we are only interested in QCD virtual corrections, only the quark line is affected, and we may adopt the result directly from the corresponding calculation in Ref. [49] for the basic photon-quark scattering diagrams in DIS. This gives

$$\hat{\sigma}^{q\to q}_{\rm NLO,vir} = \frac{C_F\alpha_s(\mu)}{2\pi}\frac{\Gamma(1-\varepsilon)^2\Gamma(1+\varepsilon)}{\Gamma(1-2\varepsilon)} \times \left(\frac{4\pi\mu^2}{-t}\right)^{\varepsilon}\left(-\frac{2}{\varepsilon^2}-\frac{3}{\varepsilon}-8\right)\hat{\sigma}^{q\to q}_{{\rm LO},\varepsilon}, \tag{8}$$

where

$$\hat{\sigma}^{q\to q}_{{\rm LO},\varepsilon} = 2\alpha_{\rm em}^2 e_q^2 \frac{1}{sv}\left(\frac{1+v^2}{(1-v)^2}-\varepsilon\right)\delta(1-w) \tag{9}$$

is the Born cross section computed in $4-2\varepsilon$ dimensions. Furthermore, $C_F = (N_c^2-1)/2N_c$, with N_c being the number of colors.

C. Real-emission corrections at NLO

The real diagrams have $2 \to 3$ topology. To obtain the desired contribution to an inclusive-parton cross section we need to integrate over the phase space of the lepton and the "unobserved" parton in the final state. This can be done in $4-2\varepsilon$ dimensions using the standard techniques available in the literature [50–52].

After phase space integration, the result for the real-emission contribution for the $q \to q$ channel takes the form

$$\hat{\sigma}^{q\to q}_{\rm NLO,real} = \hat{\sigma}^{q\to q}_A(v,w,\mu,\varepsilon) + \frac{\hat{\sigma}^{q\to q}_B(v,w,\mu,\varepsilon)}{(1-w)^{1+2\varepsilon}}, \tag{10}$$

where both functions $\hat{\sigma}^{q\to q}_A$ and $\hat{\sigma}^{q\to q}_B$ carry a $1/\varepsilon$ pole, but are well behaved in the limit $w \to 1$. Obviously, the second term in (10) requires special care in this limit since the denominator would lead to a nonintegrable behavior for $\varepsilon = 0$. We deal with this limit by means of the expansion

$$(1-w)^{-1-2\varepsilon} = -\frac{1}{2\varepsilon}\delta(1-w) + \frac{1}{(1-w)_+} - 2\varepsilon\left(\frac{\ln(1-w)}{1-w}\right)_+ + \mathcal{O}(\varepsilon^2), \tag{11}$$

where the plus distribution is defined in the usual way by

$$\int_0^1 dw f(w)[g(w)]_+ = \int_0^1 dw[f(w)-f(1)]g(w). \quad (12)$$

This expansion makes the singularities in $1/\varepsilon$ explicit. When combined with the pole terms in $\hat{\sigma}_B^{q\to q}$, the term $\propto \delta(1-w)$ in (11) leads to a double pole term that cancels against the double pole in the virtual correction in Eq. (8). This well-known behavior reflects the cancellation of infrared singularities in partonic observables. The channels $q \to g$ and $g \to q$ in Figs. 3(b) and 3(c) are infrared finite at NLO.

D. Collinear subtraction for parton distribution functions and fragmentation functions

After the cancellation of infrared singularities between real and virtual contribution, the partonic cross sections still exhibit single poles that reflect collinear singularities arising when an "observed" parton (either the incoming one or the one that fragments) becomes collinear with the unobserved parton. The factorization theorem states that these poles may be absorbed into the parton distribution functions or into the fragmentation functions. This procedure may be formulated in terms of *renormalized* parton densities and fragmentation functions (see, e.g., Ref. [53]). In fact, naive definitions of "bare" parton densities and fragmentation functions contain ultraviolet singularities that can be dealt with as well by using dimensional regularization. At NLO, the corresponding ultraviolet $1/\varepsilon$ poles that appear can be removed in the $\overline{\text{MS}}$ scheme by introducing renormalized functions in the form

$$f_{\text{bare}}^{q/N}(x,\mu) = f_{\text{ren}}^{q/N}(x,\mu) + \frac{\alpha_s(\mu)}{2\pi}\frac{S_\varepsilon}{\varepsilon}(P_{qq}\otimes f_{\text{ren}}^{q/N})(x,\mu) + \frac{\alpha_s(\mu)}{2\pi}\frac{S_\varepsilon}{\varepsilon}(P_{qg}\otimes f_{\text{ren}}^{g/N})(x,\mu) + \mathcal{O}(\alpha_s^2), \quad (13)$$

$$D_{\text{bare}}^{h/q}(z,\mu) = D_{\text{ren}}^{h/q}(z,\mu) + \frac{\alpha_s(\mu)}{2\pi}\frac{S_\varepsilon}{\varepsilon}(P_{qq}\otimes D_{\text{ren}}^{h/q})(z,\mu) + \frac{\alpha_s(\mu)}{2\pi}\frac{S_\varepsilon}{\varepsilon}(P_{gq}\otimes D_{\text{ren}}^{g/N})(z,\mu) + \mathcal{O}(\alpha_s^2), \quad (14)$$

where we have the usual splitting functions

$$P_{qq}(y) = C_F\left[\frac{1+y^2}{(1-y)_+} + \frac{3}{2}\delta(1-y)\right], \quad (15)$$

$$P_{qg}(y) = T_R[y^2+(1-y)^2], \quad (16)$$

$$P_{gq}(y) = C_F\frac{1+(1-y)^2}{y}, \quad (17)$$

(with $T_R = 1/2$), and where the $\otimes$ symbol indicates the convolution

$$(P\otimes f)(x) \equiv \int_x^1 \frac{dy}{y}P(y)f\left(\frac{x}{y}\right). \quad (18)$$

The constant $S_\varepsilon \equiv (4\pi)^\varepsilon/\Gamma(1-\varepsilon)$ in (13) and (14) corresponds to the usual $\overline{\text{MS}}$ scheme. Inserting the bare distributions into the LO expression for the hadronic cross section, we obtain additional $\mathcal{O}(\alpha_s\alpha_{\text{em}}^2)$ contributions. These precisely cancel the collinear poles associated with the observed partons in the NLO partonic cross sections, for all three channels.

Even after this procedure, one type of collinear singularity remains. It is generated by a momentum configuration where the exchanged photon is collinear to the incoming lepton. As discussed at the beginning of this section, the presence of this singularity is an artifact of neglecting the lepton's mass. In the following two subsections we discuss our treatment of this issue.

E. Weizsäcker-Williams contribution

One approach for dealing with the collinear lepton singularity is to introduce bare and renormalized QED parton distributions for the lepton, very analogous to the procedure that we discussed in the previous section for the nucleon's parton distributions. The only differences are that for leptons the partons are the lepton itself and the photon, and that we can safely compute their distributions in QED perturbation theory. To lowest order in QED, we just have $f^{\ell/\ell}(y) = \delta(1-y)$, corresponding to the Born contribution in Fig. 1. The hard process involving an incoming lepton will always require two electromagnetic interactions and hence be of order α_{em}^2, as seen explicitly in Eq. (4). This is different for a hard process with an incoming photon such as $\gamma q \to qg$, which is of order $\alpha_{\text{em}}\alpha_s$. This implies that at NLO in QCD (at order $\alpha_{\text{em}}^2\alpha_s$) there will be contributions generated by the photon acting as a parton of the lepton and participating in the hard process. A generic picture for such types of contributions, known as Weizsäcker-Williams contributions, is shown in Fig. 4. In essence, the lepton merely serves as a source of real photons for the contributions shown in the figure. Like its nucleon counterpart, the corresponding photon-in-lepton distribution $f^{\gamma/\ell}(y)$ will require renormalization. Following (13) we may write

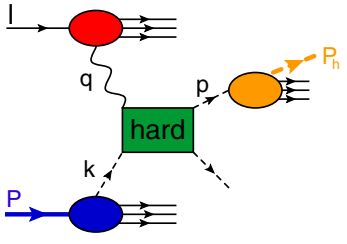

FIG. 4 (color online). General Weizsäcker-Williams contribution at NLO. The quasireal photon entering the hard scattering part is treated as a parton in the lepton.

$$f^{\gamma/\ell}_{\text{bare}}(y,\mu) = f^{\gamma/\ell}_{\text{ren}}(y,\mu) + \frac{\alpha_{\text{em}}}{2\pi}\frac{S_\varepsilon}{\varepsilon}(P_{\gamma\ell} \otimes f^{\ell/\ell}_{\text{ren}})(y,\mu) + \ldots \tag{19}$$

where $P_{\gamma\ell} = P_{gq}/C_F$ and the ellipses denote a term involving a photon-to-photon splitting that makes contributions beyond the order in α_{em} we consider here. Within the same reasoning, we can set $f^{\ell/\ell}_{\text{ren}}(y) = \delta(1-y)$ in (19).

The bare photon-in-lepton distribution $f^{\gamma/\ell}_{\text{bare}}$ in Eq. (19) can be defined analogously to the gluon distribution in a nucleon in terms of the matrix element (see also [6])

$$\begin{aligned}\Omega^{\mu\nu}(y) &\equiv n_\rho n_\sigma \int_{-\infty}^{\infty}\frac{d\lambda}{2\pi y}\,\mathrm{e}^{i\lambda y}\langle \ell|F^{\sigma\nu}_{\text{em}}(0)U[0;\lambda n]F^{\rho\mu}_{\text{em}}(\lambda n)|\ell\rangle, \\ &= \frac{-g^{\mu\nu}_\perp}{2(1-\varepsilon)} f^{\gamma/\ell}_{\text{bare}}(y,\mu).\end{aligned} \tag{20}$$

In this definition n is a light-cone vector conjugate to the lepton momentum l, with $n^2 = 0$ and $l\cdot n = 1$. Furthermore, $F^{\mu\nu}_{\text{em}} = \partial^\mu A^\nu - \partial^\nu A^\mu$ is the electromagnetic field-strength tensor, and we have inserted a (straight) Wilson line $U[0;\lambda n]$ that ensures the electromagnetic gauge invariance of the matrix element. The transverse projector in (20) is given as $g^{\mu\nu}_\perp = g^{\mu\nu} - l^\mu n^\nu - l^\nu n^\mu$.

Since the matrix element in (20) contains electromagnetic fields and elementary leptons in the in- and out-states we can compute it to LO in QED. In this calculation we keep a nonvanishing lepton mass m_ℓ in order to obtain an infrared-finite result. To order $\mathcal{O}(\alpha_{\text{em}})$ we find,

$$f^{\gamma/\ell}_{\text{bare}}(y,\mu) = \frac{\alpha_{\text{em}}}{2\pi}P_{\gamma\ell}(y)S_\varepsilon\left[\frac{1}{\varepsilon} + \ln\left(\frac{\mu^2}{y^2 m_\ell^2}\right) - 1\right] + \mathcal{O}(\alpha_{\text{em}}^2), \tag{21}$$

where, as before, $S_\varepsilon \equiv (4\pi)^\varepsilon/\Gamma(1-\varepsilon)$. In close analogy to parton distributions of the nucleon we can perform an $\overline{\text{MS}}$ renormalization of the distribution and obtain

$$\begin{aligned}f^{\gamma/\ell}_{\text{ren}}(y,\mu) &= f^{\gamma/\ell}_{\text{bare}}(y,\mu) - \frac{\alpha_{\text{em}}}{2\pi}P_{\gamma\ell}(y)\frac{S_\varepsilon}{\varepsilon} + \mathcal{O}(\alpha_{\text{em}}^2) \\ &= \frac{\alpha_{\text{em}}}{2\pi}P_{\gamma\ell}(y)\left[\ln\left(\frac{\mu^2}{y^2 m_\ell^2}\right) - 1\right] + \mathcal{O}(\alpha_{\text{em}}^2).\end{aligned} \tag{22}$$

This renormalized distribution is closely related to the "classic" Weizsäcker-Williams distribution [44–47]. The logarithm in (22) may be derived from an integration over the photon's virtuality $-q^2$ (where q is the photon momentum). For the standard Weizsäcker-Williams distribution one performs this integration from the lower kinematic limit $m_\ell^2 y^2/(1-y)$ to an upper limit Q^2_{max} fixed by the experimental condition imposed on the scattered lepton. This gives rise to a term $\frac{\alpha_{\text{em}}}{2\pi}P_{\gamma\ell}(y)\ln(Q^2_{\text{max}}(1-y)/(y^2 m_\ell^2))$ in the photon spectrum, which can be recovered by an appropriate choice of the scale μ in (22).

For the contribution related to $f^{\gamma/\ell}_{\text{ren}}$ the photon virtuality is then neglected everywhere else in the hard scattering. One thus considers scattering diagrams with a real incoming photon. We thus write the generic factorized cross section for the contribution as

$$\begin{aligned}E_h\frac{d^3\sigma^{\ell N\to hX}_{\text{WW}}}{d^3P_h} = \frac{1}{S}\sum_{i,f}\int_0^1\frac{dx}{x}\int_0^1\frac{dz}{z^2}\int_0^1 dy\,\delta\left(y + \frac{t}{s+u}\right) \\ \times f^{i/N}(x,\mu)D^{h/f}(z,\mu)f^{\gamma/\ell}_{\text{ren}}(y,\mu)\hat{\sigma}^{\gamma i\to f},\end{aligned} \tag{23}$$

with the cross sections $\hat{\sigma}^{\gamma i\to f}$ describing the scattering $\gamma i \to fx$ of the photon off parton i in the nucleon (to be given below). At $\mathcal{O}(\alpha_s)$ we encounter three channels with an incoming photon: $\gamma q \to q(g)$, $\gamma q \to g(q)$, and $\gamma g \to q(\bar{q})$ (the partons in parentheses are not observed). The relevant diagrams are as shown in Figs. 3(a)–3(c), but with the lepton lines removed and the virtual photon replaced by a real photon. Being $2\to 2$ diagrams, their calculation is straightforward. Inserting now the bare WW distribution we generate precisely the pole terms required to cancel the lepton collinear divergences discussed at the end of Sec. II D. This happens in the same way for all partonic channels. We note that the dependence on the scale μ associated with the lepton also disappears. This has to be the case, since for a finite lepton mass there would never be any lepton collinear divergences in the first place.

F. Calculation with $m_\ell \neq 0$

As we noted earlier, the presence of collinear singularities associated with lepton-photon splitting is really an artifact of neglecting the lepton's mass. In principle we should therefore perform a full calculation in which the lepton's mass is kept finite. This is trivial for the virtual diagrams, since the QCD corrections do not affect the lepton line. However, inclusion of a lepton mass considerably complicates the phase space integrations for the real diagram. Nevertheless, it is possible to compute the relevant integrals using the results given in Ref. [51]. One may then expand the result in powers of the lepton mass and neglect terms suppressed by powers of $\mathcal{O}(m_\ell)$. In this way, the "would-be" collinear singularity is regularized by the lepton mass and shows up as a term $\sim\ln(m_\ell^2)$. Terms independent of m_ℓ are also kept. All other parts of the calculation proceed as before, and the partonic cross section thus has the structure

$$\begin{aligned}\hat{\sigma}^{i\to f}_{\text{NLO}}(v,w,m_\ell,\mu) &= \hat{\sigma}^{i\to f}_{\log}(v,w,\mu)\ln(m_\ell^2/s) \\ &\quad + \hat{\sigma}^{i\to f}_0(v,w,\mu) + \mathcal{O}(m_\ell^2\ln(m_\ell^2)).\end{aligned} \tag{24}$$

for each channel.

We have checked explicitly for all three channels that our two approaches for treating the initial lepton are equivalent:

The full result obtained using the WW contribution in the previous subsection agrees with that for $m_\ell \neq 0$, as long as we only keep the leading terms as discussed in Eq. (24). The equivalence of the two approaches serves as an important check of our calculation and also explicitly demonstrates the universality of the WW distribution.

G. Final results for single-inclusive hadron production

We now present our final results for the full partonic cross sections in analytic form. Combining the cross section (6) for massless leptons with the Weizsäcker-Williams contribution (23), we may write the full NLO cross section as

$$E_h\frac{d^3\sigma^{\ell N\to hX}}{d^3P_h}=\left(\frac{-U}{S^2}\right)\sum_{i,f}\int_{\frac{U}{T+U}}^{1+\frac{T}{S}}\frac{dv}{v(1-v)}\int_{\frac{1-vU}{v\,T}}^{1}\frac{dw}{w^2}H^{if}(v,w)\left[\hat{\sigma}_{\rm LO}^{i\to f}(v)+\frac{\alpha_s(\mu)}{\pi}\hat{\sigma}_{\rm NLO}^{i\to f}(v,w,\mu)+f_{\rm ren}^{\gamma/\ell}\left(\frac{1-v}{1-vw},\mu\right)\frac{\alpha_s(\mu)}{\pi}\hat{\sigma}_{\rm LO}^{\gamma i\to f}(v,w)\right],\tag{25}$$

where $H^{if}(v,w)$ has been defined in Eq. (7). The LO contribution, present only for the channel $q\to q$ with an incoming quark that also fragments, was already given in (4). For the NLO term in this channel we find

$$\begin{aligned}\hat{\sigma}_{\rm NLO}^{q\to q}(v,w,\mu)=\frac{\alpha_{\rm em}^2e_q^2C_F}{svw}\Bigg[&A_0^{q\to q}\delta(1-w)+A_1^{q\to q}\left(\frac{\ln(1-w)}{1-w}\right)_+\\&+\frac{1}{(1-w)_+}\left\{B_1^{q\to q}\ln\left(\frac{1-v}{v(1-v(1-w))}\right)+B_2^{q\to q}\ln(1-v(1-w))+B_3^{q\to q}\ln\left(\frac{sv^2}{\mu^2}\right)\right\}\\&+C_1^{q\to q}\ln(v(1-w))+C_2^{q\to q}\ln\left(\frac{(1-v)w}{1-vw}\right)+C_3^{q\to q}\ln\left(\frac{1-v}{(1-vw)(1-v(1-w))}\right)\\&+C_4^{q\to q}\ln\left(\frac{s}{\mu^2}\right)+C_5^{q\to q}\Bigg],\end{aligned}\tag{26}$$

where the coefficients $A_i^{q\to q}$, $B_i^{q\to q}$, $C_i^{q\to q}$ are functions of v and w and may be found in the Appendix. The channels $q\to g$ and $g\to q$ have simpler expressions:

$$\begin{aligned}\hat{\sigma}_{\rm NLO}^{q\to g}(v,w,\mu)=\frac{\alpha_{\rm em}^2e_q^2C_F}{svw}\Bigg[&C_1^{q\to g}\ln(1-v(1-w))\\&+C_2^{q\to g}\ln\left(\frac{1-v}{(1-vw)(1-v(1-w))}\right)\\&+C_3^{q\to g}\ln\left(\frac{v(1-w)s}{\mu^2}\right)+C_4^{q\to g}\Bigg],\end{aligned}\tag{27}$$

$$\begin{aligned}\hat{\sigma}_{\rm NLO}^{g\to q}(v,w,\mu)=\frac{\alpha_{\rm em}^2e_q^2T_R}{svw}\Bigg[&C_1^{g\to q}\ln\left(\frac{(1-v)w}{1-vw}\right)\\&+C_2^{g\to q}\ln\left(\frac{v(1-w)s}{\mu^2}\right)+C_3^{g\to q}\Bigg].\end{aligned}\tag{28}$$

The coefficients $C_i^{q\to g}$ and $C_i^{g\to q}$ are again given in the Appendix.

We finally list the partonic cross sections for the Weizsäcker-Williams contributions:

$$\begin{aligned}\hat{\sigma}_{\rm LO}^{\gamma q\to q}(v,w)&=\frac{C_F\alpha_{\rm em}e_q^2}{2s(1-v)}\frac{1+v^2w^2}{vw},\\\hat{\sigma}_{\rm LO}^{\gamma q\to g}(v,w)&=\frac{C_F\alpha_{\rm em}e_q^2}{2s(1-v)}\frac{1+(1-vw)^2}{1-vw},\\\hat{\sigma}_{\rm LO}^{\gamma g\to q}(v,w)&=\frac{T_R\alpha_{\rm em}e_q^2}{2s(1-v)}\frac{v^2w^2+(1-vw)^2}{vw(1-vw)}.\end{aligned}\tag{29}$$

H. Single-inclusive jet production

Having computed the inclusive hadron production cross section at NLO the extension to single-inclusive jet production is straightforward. The cross section for $\ell N\to {\rm jet}X$ may be written as

$$E_{\rm J}\frac{d^3\sigma^{\ell N\to {\rm jet}X}}{d^3P_{\rm J}}=\frac{1}{S}\sum_i\int_{\frac{-U}{S+T}}^1\frac{dw}{w}f^{i/N}\left(x=\frac{-U}{w(S+T)},\mu\right)\times\hat{\sigma}^{i\to{\rm jet}}\left(v=1+\frac{T}{S},w,\mu;R\right),\tag{30}$$

where $E_{\rm J}$ and $\vec{P}_{\rm J}$ are the energy and three-momentum of the jet and the hadronic Mandelstam variables are defined as before, now in terms of the jet momentum. The form of this expression follows from (6) by setting the fragmentation functions to $\delta(1-z)$. Of course, beyond LO, the partonic cross sections $\hat{\sigma}^{i\to{\rm jet}}$ for jet production differ from the ones for single-inclusive hadron production. This is evident from

the fact that the latter are computed as "inclusive-parton" cross sections $\hat{\sigma}^{i\to f}$ which, as we saw in Sec. II D, require collinear subtraction. This is in contrast to a jet cross section which is by itself infrared safe, as far as the final state is concerned. Instead, it depends on the algorithm adopted to define the jet, as we have indicated by the dependence on a generic jet (size) parameter R in (30).

As was discussed in Refs. [54–56], even at NLO one may still go rather straightforwardly from the single-inclusive parton cross sections $\hat{\sigma}^{i\to f}$ to the $\hat{\sigma}^{i\to\text{jet}}$, for any infrared-safe jet algorithm. The key is to properly account for the fact that at NLO two partons can fall into the same jet, so that the jet needs to be constructed from both. In fact, assuming the jet to be relatively narrow, one can determine the relation between $\hat{\sigma}^{i\to f}$ and $\hat{\sigma}^{i\to\text{jet}}$ analytically [54]. This "narrow jet approximation" (NJA) formally corresponds to the limit $R\to 0$ but turns out to be accurate even at values $R\sim 0.4$–0.7 relevant for the experiments. We follow this approach in this work. In the NJA, the structure of the NLO jet cross section is of the form $\mathcal{A}\log(R)+\mathcal{B}$; corrections to this are of $\mathcal{O}(R^2)$ and are neglected. We note that to the order $\alpha_{\text{em}}^2\alpha_s$ we consider in this paper, the Weizsäcker-Williams terms only contribute to the R-independent piece $\mathcal{B}$. This is because for almost real exchanged photons it is at this order not possible to have two coalescing partons in the final state.

III. NUMERICAL RESULTS

We now present phenomenological results for the NLO single-inclusive pion production cross section in lepton-proton scattering. As mentioned before, data on the transverse single-spin asymmetry for this reaction have been released by HERMES [2] and the Jefferson Lab Hall A Collaboration [4]. Unfortunately, corresponding cross sections were not presented, and we will therefore provide predictions for these. Furthermore, we will also present predictions for COMPASS at CERN, for a future EIC, and for experiments at Jefferson Lab after the CEBAF upgrade to 12 GeV beam energy. Finally, at the end of this section we show some phenomenological results for the inclusive production of jets at the EIC.

As we saw in the previous subsections [see Eq. (25)], our NLO result can be formulated in such a way that it contains contributions involving the photon-in-lepton distribution $f_{\text{ren}}^{\gamma/\ell}$ and LO photon-parton cross sections. These represent the contributions by quasireal photons to the cross section. An interesting question is whether this part of the cross section dominates the NLO corrections, at least for a suitable choice of the scale μ in (22). We recall that the logarithm in (22) may be obtained by an integration over the photon's virtuality where only the $1/q^2$ propagator is kept for the photon, while q^2 is neglected everywhere else in the hard scattering. We now consider the cross section

$$E_h\frac{d^3\sigma^{\ell N\to hX}}{d^3P_h}=\left(\frac{-U}{S^2}\right)\sum_{i,f}\int_{\frac{U}{T+U}}^{1+\frac{T}{S}}\frac{dv}{v(1-v)}\int_{\frac{1-vU}{v\,T}}^{1}\frac{dw}{w^2}H^{if}(v,w)\left[\hat{\sigma}_{\text{LO}}^{i\to f}(v)+f_{\text{ren}}^{\gamma/\ell}\left(\frac{1-v}{1-vw},\mu_0\right)\frac{\alpha_s(\mu)}{\pi}\hat{\sigma}_{\text{LO}}^{\gamma i\to f}(v,w)\right],\quad(31)$$

which essentially corresponds to the full NLO one in (25), but with the terms $\hat{\sigma}_{\text{NLO}}^{i\to f}$ dropped. In other words, we use the LO term and add the Weizsäcker-Williams contribution. For the latter, we choose the upper limit on $\sqrt{-q^2}$ in the photon spectrum as a large scale in the problem, $\mu_0\sim P_{h\perp}$ or even $\mu_0\sim\sqrt{S}/2$. This constitutes an attempt to obtain an approximation to the full NLO correction by assuming that the $1/q^2$ behavior of the hard cross sections is valid over most of the kinematical regime. In our studies we examine in this way the importance of the Weizsäcker-Williams contribution. As discussed in the Introduction, *if* the contribution plays a dominant role for the NLO corrections, this opens the door to approximate NLO calculations also for the spin-dependent case.

For all our calculations we use the CTEQ6.6M [57] set of parton distribution functions and the fragmentation functions of [58].

A. HERMES

Figures 5(a) and 5(b) present our results for π^+ production at HERMES at $\sqrt{S}=7.25$ GeV. We fix the renormalization and factorization scales at $\mu=P_{h\perp}$. In order to match the conventions used in $pp^\uparrow\to hX$, HERMES presents the spin asymmetry results in terms of the hadron's transverse momentum $P_{h\perp}$ and Feynman's $x_F=2P_h^z/\sqrt{S}$, where P_h^z is the z component of the hadron momentum in the center-of-mass frame of the collision, and where positive x_F is counted in the direction of the lepton beam. We have

$$\frac{d^2\sigma^{ep\to\pi X}}{dx_F dP_{h\perp}}=\frac{2\pi P_{h\perp}}{\sqrt{x_F^2+x_T^2}}E_h\frac{d^3\sigma^{ep\to\pi X}}{d^3P_h},\quad(32)$$

where $x_T=2P_{h\perp}/\sqrt{S}$. The hadronic Mandelstam variables read

$$T=-\frac{S}{2}\left(\sqrt{x_F^2+x_T^2}+x_F\right),$$
$$U=-\frac{S}{2}\left(\sqrt{x_F^2+x_T^2}-x_F\right).\quad(33)$$

Figure 5(a) shows the cross section as a function of x_F, integrated over 1 GeV $< P_{h\perp} <$ 2.2 GeV. This is the only $P_{h\perp}$ bin used in Ref. [2] with $P_{h\perp}>1$ GeV. In Fig. 5(b) we

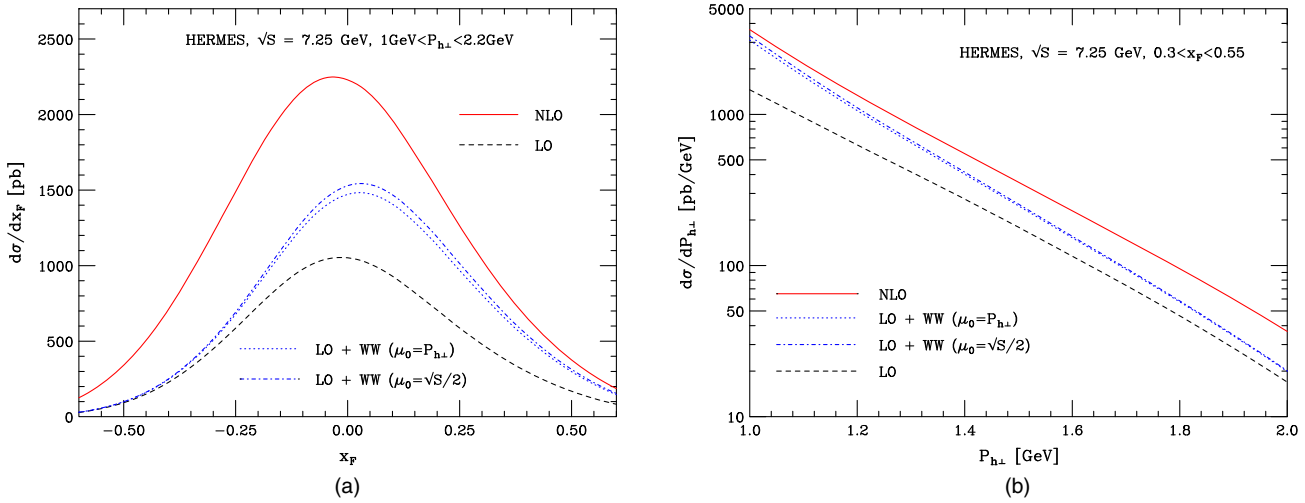

FIG. 5 (color online). Cross section for $\ell p \to \pi^+ X$ at HERMES, (a) as a function of x_F for 1 GeV $< P_{h\perp} <$ 2.2 GeV and (b) as a function of $P_{h\perp}$ for $0.3 < x_F < 0.55$. The dashed line gives the LO prediction and the solid line the NLO one. The dotted and dot-dashed lines show the approximation (31) of the NLO cross section, using $\mu_0 = P_{h\perp}$ and $\mu_0 = \sqrt{S}/2$, respectively.

examine the $P_{h\perp}$ dependence of the cross section for $0.3 < x_F < 0.55$. In both cases we find large NLO corrections; the NLO cross section is almost twice as large as the LO one. As discussed above, we also examine in how far the Weizsäcker-Williams contribution drives the NLO corrections, using Eq. (31) with $\mu_0 = P_{h\perp}$ (dotted) and $\mu_0 = \sqrt{S}/2$ (dot dashed). As one can see from the figures, the Weizsäcker-Williams contribution does lead to an increase over LO, but provides only about 50% to 70% of the NLO correction. This is likely to be attributed to the fact that the overall c.m. energy is rather low. The result with $\mu_0 = \sqrt{S}/2$ provides a slightly better description of the full NLO, although the differences are minor. We note that the WW approximation appears to work better for smaller transverse hadron momenta $P_{h\perp}$ and for larger x_F. The latter feature perhaps is at first sight surprising since positive x_F of the hadron imply on average backward scattering of the lepton, whereas the WW approximation should work better if the lepton is scattered in the forward direction. One can roughly understand this shift of the WW approximation towards positive x_F from the fact that $|T| \gg |U|$ for $x_F \to 1$ in Eq. (33). Since the dominant real-photon process $\gamma q \to q(g)$ in (29) has a $1/su$ behavior in contrast to the $1/t^2$ behavior of the LO process, the WW approximation favors the region $x_F > 0$. The full NLO partonic cross section inherits the $1/t^2$ behavior of the LO one, so that the Weizsäcker-Williams contribution can approximate it well only for $x_F > 0$.

B. Scattering with the 12 GeV beam at the Jefferson Lab

Our NLO predictions for the cross section for $\ell^3\mathrm{He} \to \pi^+ X$ in 12 GeV scattering at the Jefferson Lab are shown in Figs. 6(a) and 6(b). For the x_F distribution on the left we have assumed a fixed transverse momentum $P_{h\perp} =$ 1.5 GeV. On the right we show the $P_{h\perp}$ dependence of the cross section in the region $-0.4 < x_F < 0.4$. Again, the renormalization scale is fixed to the transverse hadron momentum, $\mu = P_{h\perp}$. Note that the rather modest c.m. energy available limits the possible size of $P_{h\perp}$ severely. For collisions using the present 6 GeV beam only transverse momenta outside the hard scattering regime are possible, which is the reason why we cannot present any results for this case.

We again observe in Figs. 6(a) and 6(b) that the NLO corrections are very large. The Weizsäcker-Williams contribution is clearly insufficient to match the NLO result here.

C. COMPASS

The results of our NLO analysis for COMPASS kinematics are shown in Figs. 7(a) and 7(b). COMPASS uses a muon beam with energy 160 GeV, resulting in $\sqrt{S} = 17.4$ GeV. Following the choice made by COMPASS, we use here the c.m. pseudorapidity η of the produced hadron rather than its Feynman x_F. Pseudorapidity is counted as positive in the forward direction of the incident muon. We have

$$\frac{d^2\sigma^{\mu p\to\pi^0 X}}{d\eta dP_{h\perp}} = 2\pi P_{h\perp} E_h \frac{d^3\sigma^{\mu p\to\pi^0 X}}{d^3P_{h\perp}}, \tag{34}$$

where the hadronic Mandelstam variables read

$$T = -P_{h\perp}\sqrt{S}e^{+\eta},$$
$$U = -P_{h\perp}\sqrt{S}e^{-\eta}. \tag{35}$$

The COMPASS spectrometer roughly covers the region $-0.1 < \eta < 2.38$. From the η dependence shown in Fig. 7(a)

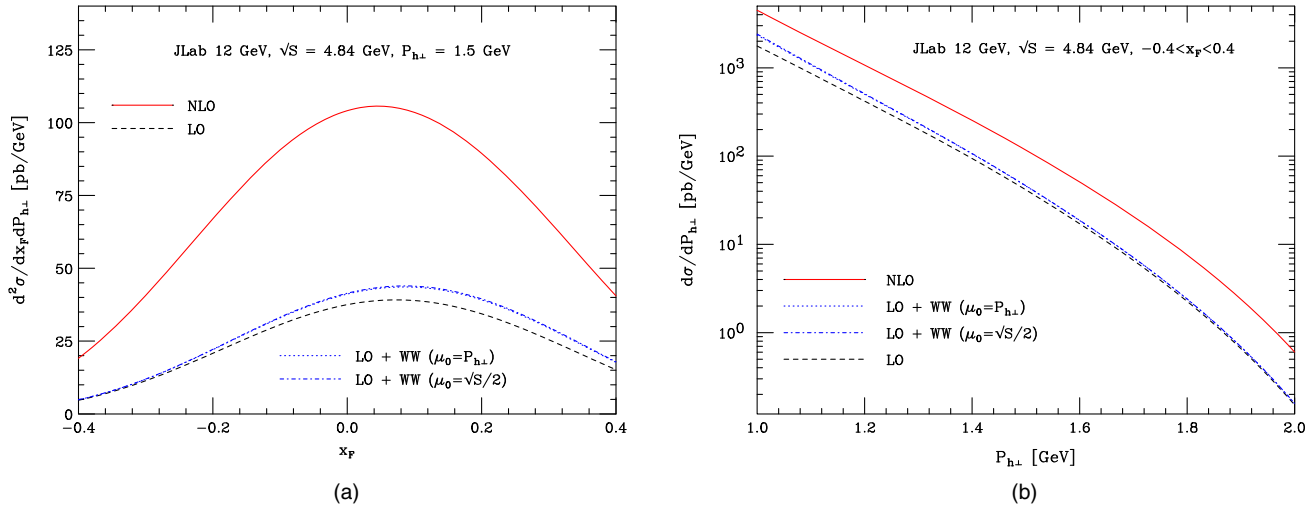

FIG. 6 (color online). Same as Figs. 5(a) and 5(b), but for ℓ^3He scattering at beam energy 12 GeV after the CEBAF upgrade at Jefferson Lab. For the cross section as a function of x_F we have used a fixed $P_{h\perp} = 1.5$ GeV, while for the $P_{h\perp}$ dependence we have integrated over $-0.4 \le x_F \le 0.4$.

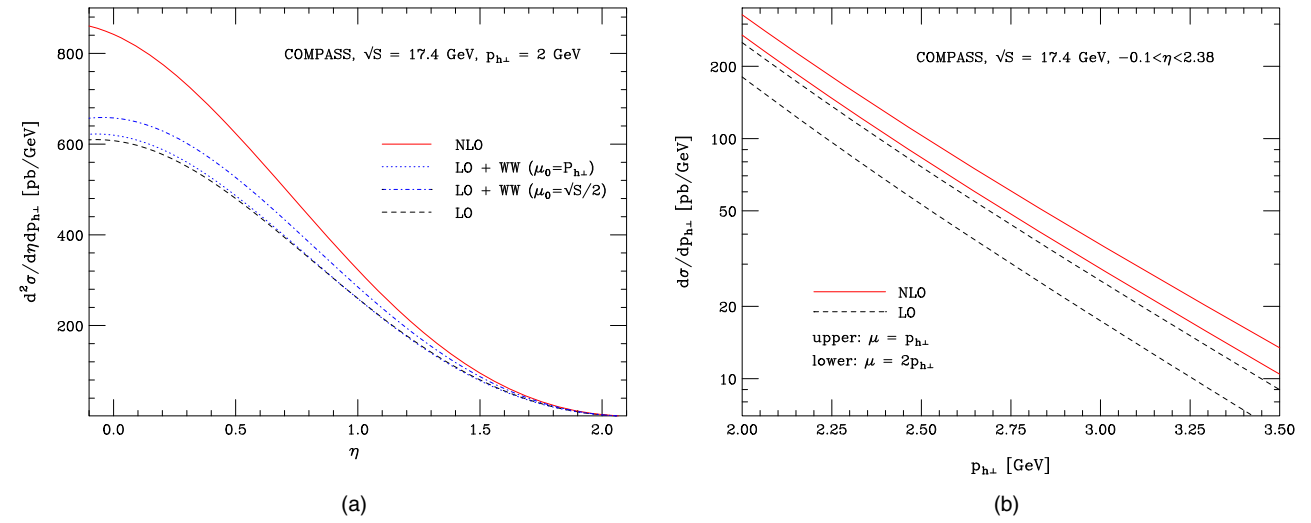

FIG. 7 (color online). Cross section for $\mu p \to \pi^0 X$ at COMPASS, (a) as a function of hadron pseudorapidity for fixed $P_{h\perp} = 2$ GeV and (b) as a function of $P_{h\perp}$ for $-0.1 \le \eta \le 2.38$. As before, the solid lines give the NLO results and the dashed lines the LO ones. The dotted and dot-dashed lines show the approximation (31) of the NLO cross section, using $\mu_0 = P_{h\perp}$ and $\mu_0 = \sqrt{S}/2$, respectively. In (b) we also present the LO and NLO results for the scale $\mu = 2P_{h\perp}$.

for a fixed transverse momentum $P_{h\perp} = 2$ GeV we observe that the NLO corrections are significant but not as large as for HERMES and JLab. They amount to an increase over LO of roughly 30%–40%. Strikingly, the Weizsäcker-Williams contribution is very small here, even for the choice $\mu_0 = \sqrt{S}/2$. This may be understood from the fact that the muon mass is about 200 times larger than the electron mass, resulting in a much smaller logarithm in the expression (22) for the photon spectrum, which then is largely canceled by the nonlogarithmic term.

For the $P_{h\perp}$ spectrum shown in Fig. 7(b) we also show the results for a different choice of the factorization and renormalization scales, $\mu = 2P_{h\perp}$. As one can see, the scale dependence decreases somewhat when going from LO to NLO but remains fairly sizable.

D. Electron-ion collider

We finally also discuss the cross section for single-inclusive pion production in electron-proton collisions at a proposed future EIC [59] with $\sqrt{S} = 100$ GeV. Thanks to the higher energy of an EIC it will become possible to probe much larger transverse hadron momenta, where pQCD is expected to work better. Figure 8(a) shows the η dependence of the cross section for a fixed transverse

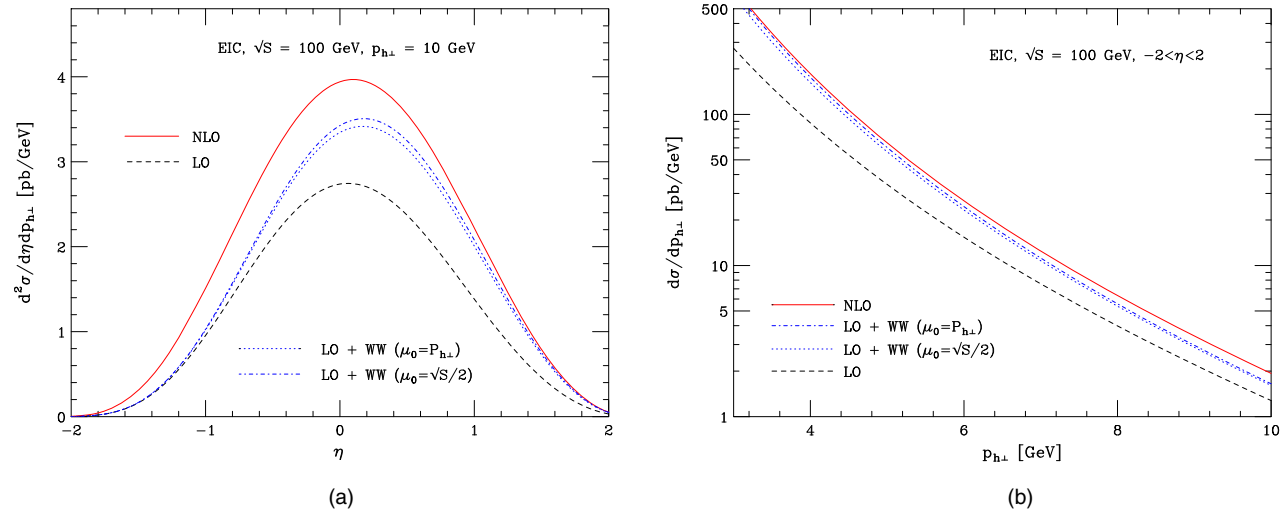

FIG. 8 (color online). Cross section for $ep \to \pi^+ X$ at an EIC with $\sqrt{S} = 100$ GeV, (a) as a function of η at fixed $p_T = P_{h\perp} = 2$ GeV and (b) as a function of $P_{h\perp}$ integrated over $|\eta| \leq 2$. The lines are as in the previous figures.

momentum $P_{h\perp} = 10$ GeV. Again we count positive η in the forward direction of the incoming lepton. The $P_{h\perp}$ dependence of the cross section is shown in Fig. 8(b), integrated over $|\eta| \leq 2$. The renormalization scale has again been fixed to the transverse hadron momentum, $\mu = P_{h\perp}$. As for COMPASS we found that the scale dependence slightly decreases for EIC kinematics when going from LO to NLO but remains relatively large.

We again find sizable NLO corrections. Overall, the Weizsäcker-Williams approximation works much better here than in the fixed-target regime. It describes the NLO cross section especially well when the hadron is produced in the electron forward direction. At midrapidity and negative rapidity the approximation tends to fall short of the full NLO result. From Fig. 8(b) we observe that the Weizsäcker-Williams also works better for smaller $P_{h\perp}$.

E. Jet production at an EIC

Given the high energy of an EIC, also jet observables will be of much interest there [6]. For example, combined analysis of data for the transverse-spin asymmetries for $ep^\uparrow \to hX$ and $ep^\uparrow \to \text{jet}X$ from a future EIC should allow for a clean separation of twist-3 parton correlations in the nucleon and in fragmentation. We therefore close this section by presenting predictions for the cross section

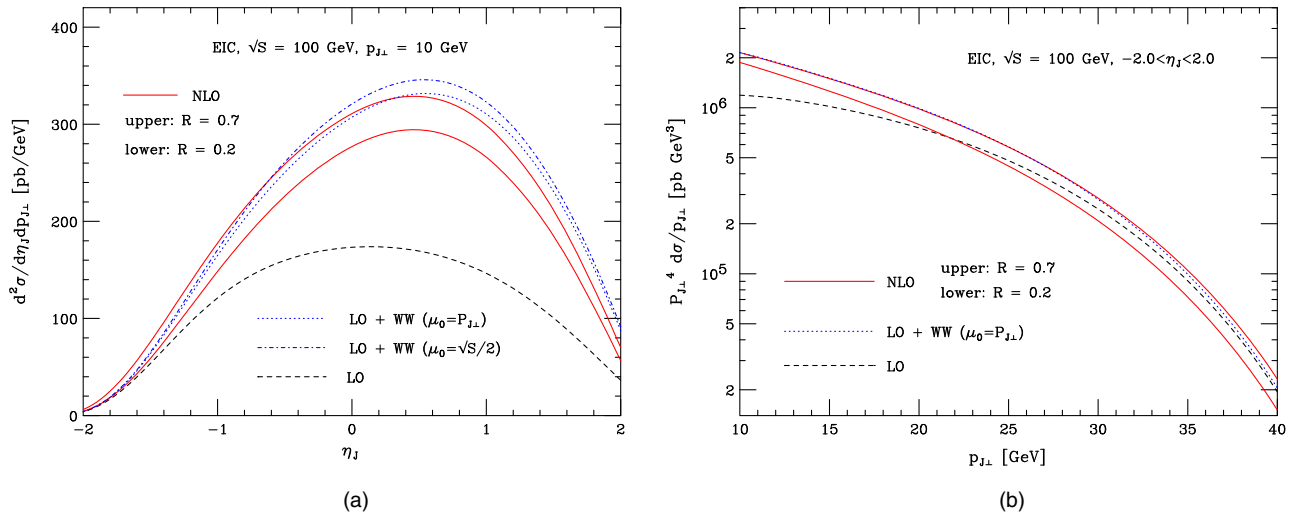

FIG. 9 (color online). Cross section for single-inclusive jet production at the EIC, (a) as a function of pseudorapidity η_J at a fixed transverse jet momentum $P_{J\perp} = 10$ GeV and (b) as a function of $P_{J\perp}$, integrated over $|\eta_J| \leq 2$. We have used the NJA [54,55] and the anti-k_t jet algorithm [60]. The solid and dotted lines show NLO predictions for two different values of the jet size parameter, $R = 0.7$ and $R = 0.2$, respectively. The dashed lines present the LO results, and the dotted ones the result for the approximation (31) of the NLO cross section, using $\mu_0 = P_{J\perp}$ and (on the left) also $\mu_0 = \sqrt{S}/2$.

for single-inclusive jet production, $ep \to \text{jet}X$. Here we use the NJA formalism outlined in Sec. II H to convert the single-hadron cross section into a jet one. We adopt the anti-k_t jet algorithm of [60]. In Fig. 9(a) we present the dependence of the cross section on the jet pseudorapidity η_J for a fixed transverse jet momentum of $P_{J\perp} = 10$ GeV. We find once again that NLO contributions are large. We also observe that, compared to the case of hadron production considered in Fig. 8(a), the NLO cross section is much more peaked in the forward electron region. The reason is that at large positive pseudorapidity $|T| \gg |U|$ in Eq. (35). Since the minimal value for the incoming parton's momentum fraction is $x_{\min} = -U/(S+T)$ in (30) rather small values of x are probed at large pseudorapidity where in turn the nucleon's parton distributions are large. On the other hand the fragmentation process suppresses the forward and backward regions in hadron production due to the large z values probed, whereas in jet production the forward electron region is enhanced due to the absence of fragmentation.

In Figs. 9(a) and 9(b), we show results for two different jet size parameters, $R = 0.7$ and $R = 0.2$. Dependence on R first occurs at NLO. As discussed at the end of Sec. II H, the first-order Weizsäcker-Williams contribution does not depend on R. It hence cannot give an accurate approximation of NLO in general. As the figure shows, the WW result happens to be rather close to the result for $R = 0.7$; this agreement, however, is essentially fortuitous.

IV. CONCLUSIONS AND OUTLOOK

We have performed next-to-leading order calculations of the partonic cross sections for the processes $\ell N \to hX$ and $\ell N \to \text{jet}X$, for which the scattered lepton in the final state is not detected. We have derived our results for a finite lepton mass, neglecting terms that are suppressed as powers of the mass over a hard scale. The results have been obtained in two ways. We have first set the mass to zero. We have regularized the ensuing collinear singularity in dimensional regularization and then subtracted it by introducing a Weizsäcker-Williams type photon distribution in the lepton. The latter can be computed in QED perturbation theory and effectively reinstates the leading lepton mass dependence, which is logarithmic plus constant. In the second approach, we have kept the lepton mass in the calculation directly, expanding all phase space integrals in such a way that the leading mass dependence is obtained. Both approaches give the same result.

We have presented phenomenological NLO predictions for various experimental setups, from fixed-target experiments (HERMES, JLab, COMPASS) to collider experiments at an EIC. We have found that the NLO corrections are large. We note that in the fixed-target regime the bulk of the corrections comes from the plus distribution terms in Eq. (26), especially at negative x_F or rapidity. As is well known, the distributions are associated with the emission of soft gluons. Since they recur with increasing power at every higher order of perturbation theory, it may be worthwhile for future work to address their resummation to all orders, similar to what was done for the photoproduction case $\ell N \to \ell' hX$ in [61].

The rather large size of the corrections that we find suggests that also the cross section with transverse polarization of the initial nucleon may be subject to large NLO corrections. This would likely have ramifications for analyses of spin asymmetry data for $\ell N^\uparrow \to hX$ in terms of twist-3 parton correlation functions. As full NLO calculations for transverse single-spin observables are difficult, we have also investigated how far it is possible to match our full NLO result for the spin-averaged cross section by adding just the Weizsäcker-Williams contribution to the LO one. We have found that this simplified approach does not appear to work well quantitatively. In other words, the NLO corrections do not appear to be dominated by quasireal photons. Nonetheless, in order to obtain a first estimate of higher-order effects for the transverse-spin asymmetry, it may be worthwhile to use the Weizsäcker-Williams contribution for the case of transversely polarized nucleons, which is much simpler to do than the full NLO calculation and was already discussed in Ref. [6].

We again emphasize that our results suggest that contributions by quasireal photons to the cross sections for the single-inclusive processes $\ell N \to hX$ and $\ell N \to \text{jet}X$ are *not* the dominant contributions, at least for large transverse hadron momenta $P_{h\perp} > 1$ GeV. In other words, an experimental setup where the final state lepton is not observed in lepton-nucleon collisions does not automatically imply that one measures an (approximated) quasireal photoproduction process. However, although quasireal photons do not dominate, they typically do play a non-negligible role for the NLO corrections. As is well known, high-energy real photons may also exhibit their own partonic structure, in which case they are referred to as "resolved" photons (see Ref. [11]). The corresponding resolved-photon contributions are formally of the same order as the Weizsäcker-Williams contribution we have considered here. They are typically suppressed in the fixed-target regime. It may be interesting to address this contribution in future work, also in order to study its impact on the transverse single-spin asymmetries. The concept of "virtual photon structure" may also prove useful in this context (see, for example, Ref. [62]).

ACKNOWLEDGMENTS

We thank A. Metz for the interesting discussions that have initiated this project, and M. Stratmann for the helpful comments. This work was supported by "Bundesministerium für Bildung und Forschung" (BMBF) Grant No. 05P12VTCTG.

APPENDIX: NLO COEFFICIENTS

Here we present the NLO coefficients in Eqs. (26), (27) and (28) for the different channels.

(a) $q \to q$ channel:

$$
\begin{aligned}
A_0^{q\to q} &= \frac{1+v^2}{(1-v)^2}\left((3+2\ln(v))\ln\left(\frac{s(1-v)}{\mu^2}\right)+\ln^2(v)-8\right),\\
A_1^{q\to q} &= 8w\frac{1+v^2}{(1-v)^2},\\
B_1^{q\to q} &= 4w\frac{1-v(1-w)+v^2(1-w(1-w))}{(1-v)^2},\\
B_2^{q\to q} &= \frac{2w}{(1-v)^2(1-v(1-w))}[(1-2v(1-w)+v^2(1-2w+2w^2)(2-2v(1-w)+v^2(1-w)^2)],\\
B_3^{q\to q} &= 4w\frac{1+v^2}{(1-v)^2}.
\end{aligned}
\tag{A1}
$$

$$
\begin{aligned}
C_1^{q\to q} &= \frac{1}{(1-v)^2(1-vw)(1-v(1-w))}[2-w-2v(1+4w)+v^2(2+9w-10w^2+w^3)-2v^3(1-w+w^2-4w^3)\\
&\quad +v^4w(2-2w-7w^2+8w^3)-2v^5w^2(1-3w+4w^2-2w^3)],\\
C_2^{q\to q} &= \frac{2(1+v^2(1+2w^2))}{(1-v)^2},\\
C_3^{q\to q} &= \frac{-2vw(3-2v(1-w)+v^2(1-2w+2w^2))}{(1-v)^2},\\
C_4^{q\to q} &= \frac{1}{(1-v)^2(1-vw)(1-v(1-w))}[2-w-2v(1+2w)+v^2(2+5w-6w^2+w^3)-2v^3(1-w+w^2-2w^3)\\
&\quad +v^4w(2-2w-3w^2+4w^3)-2v^5w^2(1-3w+4w^2-2w^3)],\\
C_5^{q\to q} &= \frac{w}{(1-v)^2(1-vw)(1-v(1-w))}[2-w-2v(2-w)+v^2(4-w-2w^2+w^3)-2v^3+v^4w(2-w^2)\\
&\quad -2v^5w^2(1-2w+2w^2-w^3)].
\end{aligned}
\tag{A2}
$$

(b) $q \to g$ channel:

$$
\begin{aligned}
C_1^{q\to g} &= \frac{2vw(1+v^2(1-w)^2)}{(1-v)^2(1-v(1-w))^2}(1-2v(1-w)+v^2(1-2w(1-w))),\\
C_2^{q\to g} &= \frac{vw(6-4vw+2v^2(1-2w(1-w)))}{(1-v)^2},\\
C_3^{q\to g} &= \frac{vw}{(1-v)^2(1-vw)^2(1-v(1-w))^2}[3-2v(3+w)+v^2(6+4w-w^2)-2v^3(3-3w+5w^2-2w^3)\\
&\quad +v^4(3-4w+5w^2-2w^3)-2v^5w(2-6w+9w^2-7w^3+2w^4)+2v^6(1-w)^2w^2(1-2w+2w^2)],\\
C_4^{q\to g} &= \frac{vw}{(1-v)^2(1-vw)^2(1-v(1-w))^2}[2-2v(5-3w)+v^2(16-3w-11w^2)-v^3(10+15w-27w^2+2w^3)\\
&\quad +v^4(2+17w-23w^2+7w^3-3w^4)-v^5w(5-5w-w^2+3w^3-2w^4)+2v^6(1-w)^2w^2(1-w+w^2)].
\end{aligned}
\tag{A3}
$$

(c) $g \to q$ channel:

$$
\begin{aligned}
C_1^{g\to q} &= \frac{2(1+v(4vw^2-2w(1+v)+v))}{(1-v)^2},\\
C_2^{g\to q} &= \frac{1}{(1-v)^2(1-vw)^2}[2(1-w+w^2)-2vw(3-2w+2w^2)+v^2(2-4w+11w^2-2w^3+2w^4)\\
&\quad -4v^3w(1-2w+3w^2)-3v^4w^2(1-2w+2w^2)],\\
C_3^{g\to q} &= \frac{1}{(1-v)^2(1-vw)^2}[1+4w-6w^2-2v(1+3w+w^2-6w^3)+v^2(1+9w+4w^2-8w^3-6w^4)\\
&\quad -v^3w(3+9w-4w^2-6w^3)+v^4w^2(1+4w-4w^2)].
\end{aligned}
\tag{A4}
$$

[1] P. L. Anthony *et al.* (E155 Collaboration), Inclusive hadron photoproduction from longitudinally polarized protons and deuterons, Phys. Lett. B **458**, 536 (1999).

[2] A. Airapetian *et al.* (HERMES Collaboration), Transverse target single-spin asymmetry in inclusive electroproduction of charged pions and kaons, Phys. Lett. B **728**, 183 (2014).

[3] C. Van Hulse (HERMES Collaboration), Recent HERMES results from inclusive and semi-inclusive hadron production, EPJ Web Conf. **85**, 02020 (2015).

[4] K. Allada *et al.* (Jefferson Lab Hall A Collaboration), Single spin asymmetries of inclusive hadrons produced in electron scattering from a transversely polarized ^{3}He target, Phys. Rev. C **89**, 042201(R) (2014).

[5] Y. Koike, Single transverse-spin asymmetry in $pp^\uparrow \to \pi X$ and $ep^\uparrow \to \pi X$, AIP Conf. Proc. **675**, 449 (2003); Single transverse spin asymmetry in $\boldsymbol{p^\uparrow p \to \pi X}$ and $\boldsymbol{ep^\uparrow p \to \pi X}$, Nucl. Phys. **A721**, C364 (2003);

[6] Z. B. Kang, A. Metz, J. W. Qiu, and J. Zhou, Exploring the structure of the proton through polarization observables in $lp \to \mathrm{jet}X$, Phys. Rev. D **84**, 034046 (2011).

[7] L. Gamberg, Z. B. Kang, A. Metz, D. Pitonyak, and A. Prokudin, Left-right spin asymmetry in $\ell N^\uparrow \to hX$, Phys. Rev. D **90**, 074012 (2014).

[8] M. Anselmino, M. Boglione, J. Hansson, and F. Murgia, Predictions for single spin asymmetries in $\ell p^\uparrow \to \pi X$ and $\gamma^* p^\uparrow \to \pi X$, Eur. Phys. J. C **13**, 519 (2000).

[9] M. Anselmino, M. Boglione, U. D'Alesio, S. Melis, F. Murgia, and A. Prokudin, Single spin asymmetries in $lp \to hX$ processes: A test of factorization, Phys. Rev. D **81**, 034007 (2010).

[10] M. Anselmino, M. Boglione, U. D'Alesio, S. Melis, F. Murgia, and A. Prokudin, Single spin asymmetries in $\ell p^\uparrow \to hX$ processes and transverse momentum dependent factorization, Phys. Rev. D **89**, 114026 (2014).

[11] For a review, see M. Klasen, Theory of hard photoproduction, Rev. Mod. Phys. **74**, 1221 (2002).

[12] For a review, see C. A. Aidala, S. D. Bass, D. Hasch, and G. K. Mallot, The spin structure of the nucleon, Rev. Mod. Phys. **85**, 655 (2013).

[13] N. Christ and T. D. Lee, Possible tests of C_{st} and T_{st} invariances in $l^\pm + N \to l^\pm + \Gamma$ and $A \to B + e^+ + e^-$, Phys. Rev. **143**, 1310 (1966).

[14] A. Metz, M. Schlegel, and K. Goeke, Transverse single spin asymmetries in inclusive deep-inelastic scattering, Phys. Lett. B **643**, 319 (2006).

[15] A. Afanasev, M. Strikman, and C. Weiss, Transverse target spin asymmetry in inclusive DIS with two-photon exchange, Phys. Rev. D **77**, 014028 (2008).

[16] A. Metz, D. Pitonyak, A. Schafer, M. Schlegel, W. Vogelsang, and J. Zhou, Single-spin asymmetries in inclusive deep inelastic scattering and multiparton correlations in the nucleon, Phys. Rev. D **86**, 094039 (2012).

[17] M. Schlegel, Partonic description of the transverse target single-spin asymmetry in inclusive deep-inelastic scattering, Phys. Rev. D **87**, 034006 (2013).

[18] K. Kanazawa, A. Metz, D. Pitonyak, and M. Schlegel, Longitudinal–transverse double-spin asymmetries in single-inclusive leptoproduction of hadrons, Phys. Lett. B **742**, 340 (2015).

[19] K. Kanazawa, A. Metz, D. Pitonyak, and M. Schlegel, Single-spin asymmetries in the leptoproduction of transversely polarized hyperons, Phys. Lett. B **744**, 385 (2015).

[20] J. W. Qiu and G. F. Sterman, Single Transverse Spin Asymmetries, Phys. Rev. Lett. **67**, 2264 (1991); Single transverse spin asymmetries in direct photon production, Nucl. Phys. **B378**, 52 (1992).

[21] Y. Kanazawa and Y. Koike, Chiral odd contribution to single transverse spin asymmetry in hadronic pion production, Phys. Lett. B **478**, 121 (2000).

[22] C. Kouvaris, J. W. Qiu, W. Vogelsang, and F. Yuan, Single transverse-spin asymmetry in high transverse momentum pion production in pp collisions, Phys. Rev. D **74**, 114013 (2006).

[23] Z. B. Kang, F. Yuan, and J. Zhou, Twist-three fragmentation function contribution to the single spin asymmetry in pp collisions, Phys. Lett. B **691**, 243 (2010).

[24] K. Kanazawa and Y. Koike, A phenomenological study on single transverse-spin asymmetry for inclusive light-hadron productions at RHIC, Phys. Rev. D **83**, 114024 (2011).

[25] H. Beppu, K. Kanazawa, Y. Koike, and S. Yoshida, Three-gluon contribution to the single spin asymmetry for light hadron production in pp collision, Phys. Rev. D **89**, 034029 (2014).

[26] A. Metz and D. Pitonyak, Fragmentation contribution to the transverse single-spin asymmetry in proton-proton collisions, Phys. Lett. B **723**, 365 (2013).

[27] F. Yuan and J. Zhou, Collins Fragmentation and the Single Transverse Spin Asymmetry, Phys. Rev. Lett. **103**, 052001 (2009).

[28] K. Kanazawa and Y. Koike, Contribution of twist-3 fragmentation function to single transverse-spin asymmetry in semi-inclusive deep inelastic scattering, Phys. Rev. D **88**, 074022 (2013).

[29] K. Kanazawa, Y. Koike, A. Metz, and D. Pitonyak, Towards an explanation of transverse single-spin asymmetries in proton-proton collisions: The role of fragmentation in collinear factorization, Phys. Rev. D **89**, 111501 (2014).

[30] M. Anselmino, M. Boglione, and F. Murgia, Single spin asymmetry for $p^\uparrow p \to \pi X$ in perturbative QCD, Phys. Lett. B **362**, 164 (1995); Phenomenology of single spin asymmetries in $\boldsymbol{p^\uparrow p \to \pi X}$, Phys. Rev. D **60**, 054027 (1999).

[31] U. D'Alesio and F. Murgia, Parton intrinsic motion in inclusive particle production: Unpolarized cross sections, single spin asymmetries and the Sivers effect, Phys. Rev. D **70**, 074009 (2004).

[32] M. Anselmino, M. Boglione, U. D'Alesio, S. Melis, F. Murgia, and A. Prokudin, Sivers effect and the single spin asymmetry A_N in $p^\uparrow p \to hX$ processes, Phys. Rev. D **88**, 054023 (2013).

[33] W. Vogelsang and F. Yuan, Next-to-leading order calculation of the single transverse spin asymmetry in the Drell-Yan process, Phys. Rev. D **79**, 094010 (2009).

[34] Z. B. Kang, I. Vitev, and H. Xing, Transverse momentum-weighted Sivers asymmetry in semi-inclusive deep inelastic scattering at next-to-leading order, Phys. Rev. D **87**, 034024 (2013); L.-Y. Dai, Z.-B. Kang, A. Prokudin, and I. Vitev, Next-to-leading order transverse momentum-weighted Sivers asymmetry in semi-inclusive deep inelastic scattering: The role of the three-gluon correlator, arXiv:1409.5851.

[35] P. Aurenche, R. Baier, A. Douiri, M. Fontannaz, and D. Schiff, Scheme invariant higher order QCD predictions for large p_t photoproduction reactions, Nucl. Phys. **B286**, 553 (1987).

[36] L. E. Gordon and J. K. Storrow, The single jet inclusive cross-section at HERA in next-to-leading order QCD, Phys. Lett. B **291**, 320 (1992); L. E. Gordon, Next-to-leading order corrections to inclusive hadron photoproduction, Phys. Rev. D **50**, 6753 (1994).

[37] D. Bödeker, Jet photoproduction at HERA in next-to-leading order QCD, Phys. Lett. B **292**, 164 (1992); QCD corrections to inclusive jet photoproduction via direct photons, Z. Phys. C **59**, 501 (1993); G. Kramer and S. G. Salesch, Single jet photoproduction at HERA in next-to-leading order QCD, Z. Phys. C **61**, 277 (1994); D. Bödeker, G. Kramer, and S. G. Salesch, Inclusive jet production at HERA: Next-to-leading order QCD corrections to the resolved and direct photon contribution, Z. Phys. C **63**, 471 (1994).

[38] M. Klasen and G. Kramer, Dijet cross sections in photon-proton collisions, Phys. Lett. B **366**, 385 (1996); Inclusive dijet production at HERA: Direct photon cross-sections in next-to-leading order QCD, Z. Phys. C **72**, 107 (1996); Inclusive two jet production at HERA: Direct and resolved cross-sections in next-to-leading order QCD, Z. Phys. C **76**, 67 (1997).

[39] S. Frixione and G. Ridolfi, Jet photoproduction at HERA, Nucl. Phys. **B507**, 315 (1997); D. de Florian and S. Frixione, Jet cross-sections in polarized photon hadron collisions, Phys. Lett. B **457**, 236 (1999); D. de Florian and W. Vogelsang, Next-to-leading order QCD corrections to inclusive hadron photoproduction in polarized lepton-proton collisions, Phys. Rev. D **57**, 4376 (1998).

[40] B. W. Harris and J. F. Owens, Photoproduction of jets at HERA in next-to-leading order QCD, Phys. Rev. D **56**, 4007 (1997); Jet photoproduction and the structure of the photon, Phys. Rev. D **57**, 5555 (1998).

[41] B. Jäger, M. Stratmann, and W. Vogelsang, Longitudinally polarized photoproduction of inclusive hadrons beyond the leading order, Phys. Rev. D **68**, 114018 (2003); Longitudinally polarized photoproduction of inclusive hadrons at fixed-target experiments, Eur. Phys. J. C **44**, 533 (2005); B. Jäger, Photoproduction of single inclusive jets at future $\boldsymbol{ep}$ colliders in next-to-leading order QCD, Phys. Rev. D **78**, 034017 (2008).

[42] Z.-B. Kang, S. Mantry, and J.-W. Qiu, N-jettiness as a probe of nuclear dynamics, Phys. Rev. D **86**, 114011 (2012); Z. B. Kang, X. Liu, S. Mantry, and J. W. Qiu, Probing nuclear dynamics in jet production with a global event shape, Phys. Rev. D **88**, 074020 (2013).

[43] Z. B. Kang, X. Liu, and S. Mantry, 1-jettiness DIS event shape: NNLL + NLO results, Phys. Rev. D **90**, 014041 (2014).

[44] C. F. von Weizsäcker, Radiation emitted in collisions of very fast electrons, Z. Phys. **88**, 612 (1934).

[45] E. J. Williams, Nature of the high-energy particles of penetrating radiation and status of ionization and radiation formulae, Phys. Rev. **45**, 729 (1934).

[46] A. C. Bawa and W. J. Stirling, Validity of the equivalent photon approximation in high-energy electron proton collisions, J. Phys. G **15**, 1339 (1989).

[47] S. Frixione, M. L. Mangano, P. Nason, and G. Ridolfi, Improving the Weizsacker-Williams approximation in electron-proton collisions, Phys. Lett. B **319**, 339 (1993).

[48] A. Afanasev, C. E. Carlson, and C. Wahlquist, Probing polarized parton distributions with meson photoproduction, Phys. Lett. B **398**, 393 (1997); Measuring polarized gluon and quark distributions with meson photoproduction, Phys. Rev. D **58**, 054007 (1998); Soft contributions to hard pion photoproduction, Phys. Rev. D **61**, 034014 (2000).

[49] G. Altarelli, R. K. Ellis, and G. Martinelli, Large perturbative corrections to the Drell-Yan process in QCD, Nucl. Phys. **B157**, 461 (1979).

[50] W. L. van Neerven, Dimensional regularization of mass and infrared singularities in two-loop on-shell vertex functions, Nucl. Phys. **B268**, 453 (1986).

[51] W. Beenakker, H. Kuijf, W. L. van Neerven, and J. Smith, QCD corrections to heavy quark production in $p\bar{p}$ collisions, Phys. Rev. D **40**, 54 (1989).

[52] L. E. Gordon and W. Vogelsang, Polarized and unpolarized prompt photon production beyond the leading order, Phys. Rev. D **48**, 3136 (1993).

[53] J. C. Collins, *Foundations of Perturbative QCD* (Cambridge University Press, Cambridge, England, 2011).

[54] B. Jäger, M. Stratmann, and W. Vogelsang, Single inclusive jet production in polarized pp collisions at $O(\alpha_s^3)$, Phys. Rev. D **70**, 034010 (2004).

[55] A. Mukherjee and W. Vogelsang, Jet production in (un) polarized pp collisions: Dependence on jet algorithm, Phys. Rev. D **86**, 094009 (2012).

[56] T. Kaufmann, A. Mukherjee, and W. Vogelsang, Next-to-leading order calculation for jets defined by a maximized jet function, Phys. Rev. D **91**, 034001 (2015).

[57] W. K. Tung, H. L. Lai, A. Belyaev, J. Pumplin, D. Stump, and C.-P. Yuan, Heavy quark mass effects in deep inelastic scattering and global QCD analysis, J. High Energy Phys. 02 (2007) 053.

[58] D. de Florian, R. Sassot, M. Epele, R. J. Hernandez-Pinto, and M. Stratmann, Parton-to-pion fragmentation reloaded, Phys. Rev. D **91**, 014035 (2015).

[59] A. Accardi, J. L. Albacete, M. Anselmino, N. Armesto, E. C. Aschenauer, A. Bacchetta, D. Boer, W. Brooks *et al.*, Electron ion collider: The next QCD frontier—understanding the glue that binds us all, arXiv:1212.1701.

[60] M. Cacciari, G. P. Salam, and G. Soyez, The anti-k_t jet clustering algorithm, J. High Energy Phys. 04 (2008) 063.

[61] D. de Florian, M. Pfeuffer, A. Schäfer, and W. Vogelsang, Soft-gluon resummation for high-p_T inclusive-hadron production at COMPASS, Phys. Rev. D **88**, 014024 (2013).

[62] M. Glück, E. Reya, and M. Stratmann, Probing the parton densities of virtual photons at ep colliders, Phys. Rev. D **54**, 5515 (1996).